

Hamiltonian Study of Improved $U(1)_{2+1}$ Lattice Gauge Theory

Mushtaq Loan,* Tim Byrnes, and Chris Hamer

School of Physics, The University of New South Wales, Sydney, NSW 2052, Australia

(Dated: June 15, 2003)

Monte Carlo results are presented, in the Hamiltonian limit, for the string tension and anti-symmetric mass gap for $U(1)$ lattice gauge theory in (2+1) dimensions, using mean-field improved anisotropic Wilson action. Evidence of scaling in the string tension and antisymmetric mass gap is observed in the weak coupling regime of the theory. The results are compared to previous simulation data using the standard Wilson action and we find that a more accurate determination of the string tension and scalar glueball masses has been achieved. The scaling behaviour observed is in good agreement with the results from other numerical calculations. Finally comparisons are made with previous estimates obtained in the Hamiltonian limit by various other studies.

PACS numbers: 11.15.Ha, 12.38.Gc, 11.15.Me

I. INTRODUCTION

Compact $U(1)$ gauge theory in (2+1) dimensions is one of the simplest models with dynamical gauge degrees of freedom and possesses some important similarities with QCD [1]. The model has two essential features in common with QCD, confinement [2, 3] and chiral symmetry breaking [4]. The theory is interesting in its own right, for it has analytically been shown to confine electrically charged particles even in the weak-coupling regime (at zero temperature) [2, 3, 5, 6, 7, 8]. The confinement is understood as a result of the dynamics of the monopoles which emerge due to the compactness of the gauge field. The string tension as a function of the coupling behaves in a similar fashion to that of the 4-dimensional $SU(N)$ lattice gauge theory. This model also allows us to work with large lattices with reasonable statistics. Other common features of compact $U(1)_{(2+1)}$ and QCD are the existence of a mass gap and of a confinement-deconfinement phase transition at some non-zero temperature. Thus, being reasonably simple and theoretically well understood in the weak-coupling limit, $U(1)$ model provides a good testing ground for the development of new methods and new algorithmic approaches.

The Hamiltonian version of the model has been studied by many methods: these include strong-coupling perturbation theory [9, 10] finite-lattice techniques [11], the t - expansions [12, 13], coupled - cluster techniques [14, 15, 16] plaquette expansions [17], quantum Monte Carlo methods [18, 19, 20] and Lanczos calculations [21, 22]. However, many of these techniques have limitations in their application to the physical systems and have shown somewhat mixed results. The plaquette expansion calculations depend on the quality of the trial wave state used. A simple trial state chosen may prove to be inadequate to explore regions of interest due to small overlap of this state with the true state of the system. The Lanczos calculations are restricted by the size of the system

and the number of the states in the basis grows rapidly as the iteration procedure proceeds, whereas series expansions rely on extrapolation procedures. The Greens Function Quantum Monte Carlo methods run into difficulties for non-Abelian models and exhibit a systematic dependence on the “trial wave function” [23, 24].

Standard Euclidean Path Integral Monte Carlo (PIMC) techniques have proved to be a powerful technique and may give better results than other weak-coupling Monte Carlo methods, even in the Hamiltonian limit. The PIMC methods has had a wide range of applications in lattice gauge and condensed matter systems. Application of this method has been extremely successful in the study of two- and three dimensional models as well as four-dimensional systems [25, 26]. The results for $U(1)$, $SU(2)$ and $SU(3)$ lattice gauge theories have given rise to great optimism about the possibility of obtaining results relevant to continuum physics from Monte Carlo simulations of lattice versions of the corresponding theory. Such an optimistic view is supported by recent work of Sexton *et al* [27], Boyd *et al* [28], Luo *et al* [29] and Morningstar and Peardon [30] who have attempted to derive masses of the low-lying hadrons from such calculations and report successful results. More recent is the application of PIMC methods to obtain the reliable results in the Hamiltonian limit for the $U(1)$ model in (2+1) dimensions [31] and $SU(3)$ lattice gauge theory in (3+1) dimensions on anisotropic lattices [32].

Lattice simulations have undergone significant changes over past few years. A major reason for these changes was the realization that the large radiative corrections occurring in many quantities in lattice theories emerge from cutoff effects due to tadpole diagrams specific to lattice actions [33]. These diagrams are induced by the nonlinear relationship between the lattice variables $U_\mu(x)$ and the gauge fields $A_\mu(x)$ of the continuum theory:

$$U_\mu(x) \equiv e^{i a g A_\mu(x)}. \quad (1)$$

The higher dimension operators in such a representation generally induce large radiative corrections. Lepage and Mackenzi [33] recognized that contributions of these lattice artifacts are only suppressed by the pow-

*Electronic address: mushe@phys.unsw.edu.au

ers of g^2 , due to the ultraviolet divergences generated by the tadpole loops, rather than powers of a . They, therefore, proposed a mean-field improvement to remove the tadpole diagrams. Mean-field theory is introduced by renormalizing the link variables: $U_i(x) \rightarrow U_i(x)/u_s$ and $U_t(x) \rightarrow U_t(x)/u_t$, where u_s and u_t are the renormalization factors for the spatial and temporal links respectively. These mean-field parameters are determined by guessing input values for use in action, measuring the mean-link in a simulation, then readjusting the input values accordingly and tuning until the input values match the measured values.

Our aim in this work is to apply standard Euclidean path integral Monte Carlo methods to the mean-field improved U(1) model in (2+1) dimensions for anisotropic lattices. Simulations over a range of anisotropies were performed, enabling reliable extrapolation to the Hamiltonian limit, in which time becomes a continuous variable. Using average plaquette tadpole renormalization scheme, we extract the estimates of the string tension and low-lying glueball masses. The mean-field improved U(1) gauge model in (2+1) dimensions is outlined in Sec. II. We present our results and discussion of the string tension and glueball measurements in Sec. III. Our conclusions are given in Sec. IV, along with the outline of future work.

II. THE MODEL

The tadpole improved U(1) gauge action in (2+1) dimensions on an anisotropic lattice [34] is defined as

$$S_G = \frac{\beta_s}{u_s^4} \sum_{r,i < j} \text{ReTr} \left(1 - P_{ij}(r) \right) + \frac{\beta_t}{u_t^2 u_s^2} \sum_{r,i} \text{ReTr} \left(1 - P_{it}(r) \right), \quad (2)$$

where $P_{\mu\nu}(r)$ is the plaquette operator in the $\mu\nu$ -plane and is defined as follows,

$$P_\mu(r) = U_\mu(r) U_\nu(r + \hat{\mu}) U_\mu^\dagger(r + \hat{\nu}) U_\nu^\dagger(r) \quad (3)$$

and u_s and u_t are the mean-field improvement factors that largely correct for the radiative corrections induced by of the higher dimension operators. In the classical limit¹

$$\begin{aligned} \beta_s &= \frac{a_t}{g^2 a} = \frac{1}{g^2} \Delta\tau \\ \beta_t &= \frac{a}{g^2 a_t} = \frac{1}{g^2} \frac{1}{\Delta\tau} \end{aligned} \quad (4)$$

where $\Delta\tau = \xi = a_t/a$ is the bare anisotropy parameter, a_t and a are temporal and spatial lattice spacings respectively. The physical anisotropy, as measured by means of spatial versus temporal correlation lengths for instance, will differ from the ‘bare’ anisotropy $\Delta\tau$. Since we are only interested in the Hamiltonian limit $\Delta\tau \rightarrow 0$, however, this is of no concern for our present results. Eq. (2) reproduces the continuum action as $a \rightarrow 0$, provided that $\beta = 1/g^2$ ($g^2 = a\epsilon^2$ in (2+1) dimensions). The mean fields u_s and u_t can be defined by using the measured values of the average plaquettes. One first computes u_s from spatial plaquettes, $u_s^4 = \langle P_{ij} \rangle$, and then u_t from temporal plaquettes, $u_t^2 u_s^2 = \langle P_{it} \rangle$. Alternatively one can use the mean links in Landau gauge [35]

$$u_t = \langle \text{ReTr} U_t \rangle, \quad u_s = \langle \text{ReTr} U_i \rangle \quad (5)$$

However, when a_t is significantly smaller than a_s , we expect the mean temporal link to be very close to unity, since in perturbation theory $1 - \langle \text{Tr} U_t \rangle \propto (a_t/a_s)^2$. As we are only interested in the Hamiltonian limit, hence we adopt the following prescription [36, 37] for the mean fields

$$u_t \equiv 1, \quad u_s = \langle P_{ij} \rangle^{1/4} \quad (6)$$

The scaling behaviour for the mass gap M obtained by weak coupling perturbation theory [3] is

$$M^2 a^2 = \beta e^{-f_0 \beta + f_1} = M_D^2 \quad (7)$$

and the string tension $K = \sigma a^2$ obeys a lower bound

$$K > \text{const.} M_D \beta^{-1} \quad (8)$$

where a is the lattice spacing and f_0, f_1 are the constant coefficients. It has been rigorously proven [8] that the model shows confinement for all values of the coupling.

III. NUMERICAL SIMULATIONS AND RESULTS

Using the anisotropic Wilson gauge action with mean field improvement, we perform path integral Monte Carlo simulations on finite lattices of size $N_s^2 \times N_t$, where N_s is the number of lattice sites in the space direction and N_t in the temporal direction, with the ratio $\Delta\tau = a_t/a$. By varying $\Delta\tau$ it is possible to change a_t , while keeping the lattice spacing in the spatial direction fixed. Gauge configurations were generated using a Metropolis algorithm. The details of the algorithm for updating are given elsewhere [31]. Configurations were generated on a $16^2 \times N_t$ ($N_t = 16 - 64$) lattices for a range of couplings $\beta = 1 - 2.5$. Configurations were selected after 50,000 thermalization sweeps. The mean link is averaged every 100 sweeps and updated during thermalization. After discarding the initial number of sweeps, the configurations were stored every 250 sweeps thereafter for later analysis. Ensembles of about 1000 configurations were

¹ In the quantum theory $\beta_s = \frac{1}{g_s^2 \xi}$, $\beta_t = \frac{1}{g_t^2} \xi$, where $g_t^2 \neq g_s^2$ if $\xi \neq 1$. Since we have taken the classical values of the couplings, $g_s^2 = g_t^2 = g_E^2$ the overall factor of $\eta = \sqrt{g_t^2/g_s^2}$ in the action has been neglected.

used to measure the string tension, while 1200 configurations were generated at each β for glueball measurements. Measurements made on these stored configurations were grouped into 5 blocks, and the mean and standard deviation of the final quantities were estimated by averaging over the block averages.

A. String Tension

The conventional method for determining the force between two static charges on the lattice is by measuring Wilson loops. We have measured Wilson loops up to sizes 8×8 and used them to estimate the static quark potential

$$V(R) = -\lim_{T \rightarrow \infty} \frac{1}{T} \ln W(R, T). \quad (9)$$

The string tension is extracted from Wilson loops by establishing the linear behaviour for the static quark potential at large separation R . We have chosen to fit our results for $V(R)$ to the form [8]

$$V(R) = a + \sigma R + b \ln R, \quad (10)$$

where the linear term dominates the behaviour at large distances and a logarithmic Coulomb term, as expected for classical QED in (2+1) dimensions, dominates the behaviour at small distances.

To obtain the estimates of the string tension in the Hamiltonian limit, an extrapolation is performed by a simple cubic fit in powers of $\Delta\tau^2$ for each β value. The errors for the extrapolation may be obtained by the “linear, quadratic, cubic” extrapolant method [38]. Figure 1 shows our estimates of the string tension as a function of the anisotropy $\Delta\tau^2$ for various fixed β values. A fairly smooth dependence of string tension with $\Delta\tau^2$ for various couplings is seen.

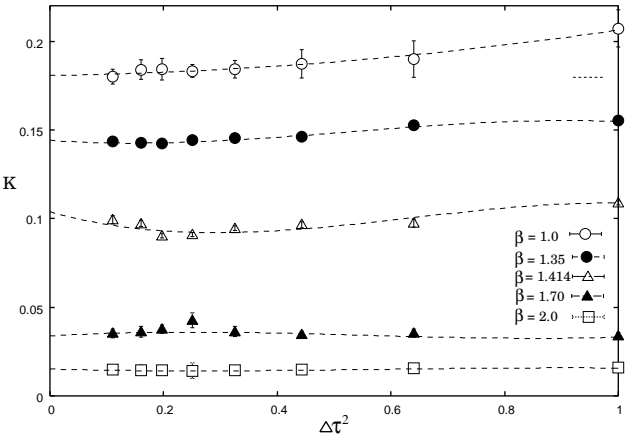


FIG. 1: Extrapolation of the string tension to the Hamiltonian limit $\Delta\tau \rightarrow 0$, for various β .

Figure 2 shows the estimates of string tension $K = \sigma a^2$, together with the results obtained using the standard Wilson action [31], as a function of β . The solid line

on the graph represents a fit to the weak-coupling asymptotic form (8). It can be seen that this form represents the data rather well in the interval $1.4 \leq \beta \leq 2.30$. The string tension exhibits scaling behaviour with the mean-field improved action whereas the results obtained using the standard Wilson action have larger show less consistent scaling behaviour. Also, in contrast with the Wilson action, a significant reduction in the errors is clearly apparent with mean-field improved action. We, however, note that the constant coefficient (intercept of the scaling curve) is still 4 times larger in magnitude than the theory predicts [8], compared to our previous estimates without tadpole improvement [31] which were estimated by a factor of 5 - 6. It is possible that the discrepancy may be due to the systematic errors, which, for the Wilson gauge action, are generally of the order a^2 with respect to the continuum limit and higher-order quantum corrections. It would be interesting to examine the scaling behaviour and sensitivity of the constant coefficient to the improved discretization. The graph also compares our results with the existing Hamiltonian results [1, 39]. It can be seen that our results are consistent with earlier Hamiltonian estimates, though less accurate in the large β region.

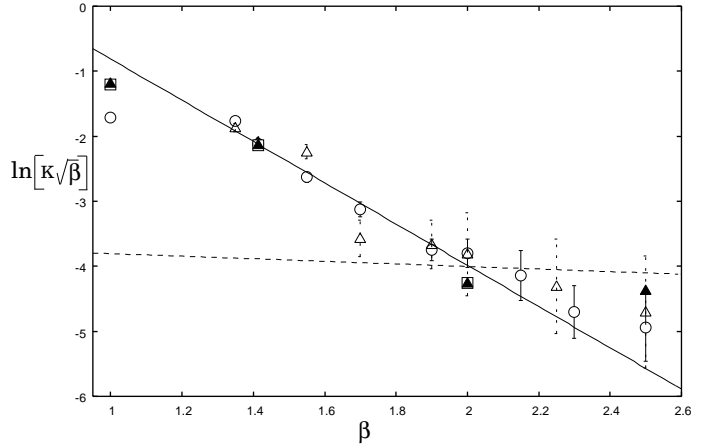


FIG. 2: The logarithm of the string tension as a function of inverse coupling. Our present estimates are shown as open circles. The solid line is the result of fitting to the form (8) for $1.4 \leq \beta \leq 2.30$. Our earlier estimates of string tension [31], using the standard Wilson action, are shown as open triangles. Earlier results from an exact linked cluster expansion [39] and quantum Monte Carlo simulations [1] are shown as solid triangles and open squares respectively. The dashed line represents the finite size behaviour [40].

The leading finite-size scaling correction to the string tension in the Hamiltonian version is found [40] to behave as

$$K = \frac{1}{2\beta L} \quad (11)$$

where $L = N_s$ is the lattice size. The dashed line in the graph represents the finite size behaviour. The plot shows that beyond $\beta = 2.15$, the string tension is consistent,

within errors, with the finite-size behaviour predicted by Eq. (11).

B. Antisymmetric Mass gap

To study the glueball correlator, it is important to use a glueball operator with strong ground state overlap. For such an operator, the signal-to-noise ratio is also optimal. Large bases of at least 27 operators were used and optimized correlators were determined by exploiting link smearing and variational techniques [37, 41].

Following Morningstar and Peardon [37] and Teper [41] we calculate an optimized correlation function,

$$C_i(\tau) = \sum_{\tau_0} \langle 0 | \bar{\Phi}_i(\tau + \tau_0) \bar{\Phi}_i(\tau_0) | 0 \rangle \quad (12)$$

where $\bar{\Phi}_i(\tau) = \Phi_i(\tau) - \langle 0 | \Phi_i(\tau) | 0 \rangle$ is the vacuum-subtracted operator capable of creating a glueball out of vacuum. The vacuum-subtraction operator is averaged over the whole ensemble before subtracting from the correlator.

The optimized correlation function was fitted with the simple form

$$C_i(\tau) = c_1 \cosh m_i \left(\frac{T}{2} - \tau \right) \quad (13)$$

to determine the glueball mass estimates. The Hamiltonian estimates of the mass gap are obtained by performing an extrapolation using a simple cubic fit in the powers of $\Delta\tau^2$ for various values of inverse coupling.

The estimates of the antisymmetric mass gap are graphed against β in Figure 3.

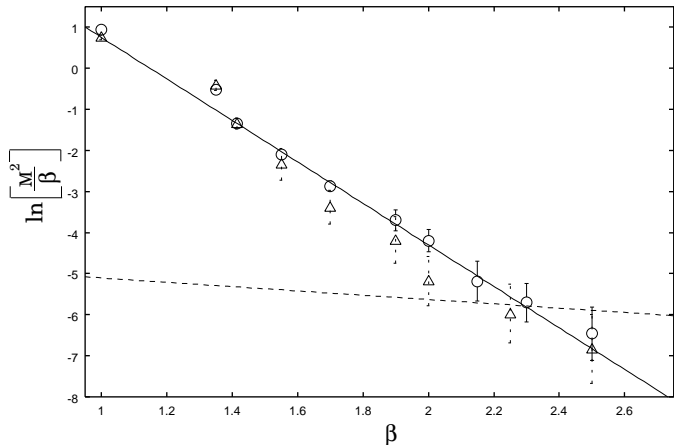


FIG. 3: The logarithm of the antisymmetric mass gap as a function of β . Open circles show our present estimates. The solid line is the fit to the data for $1.4 \leq \beta \leq 2.30$. Our previous estimates of the mass gap [31], using the standard Wilson action, are shown as open triangles. The dashed line represents the finite size effects [42].

This plot shows our present results together with our earlier results using the standard Wilson action [31]. The solid line is the result of fitting for $1.4 \leq \beta \leq 2.30$ to the form (9) to find the scaling slope and the intercept of the scaling curve. Our results for these coefficients are shown and compared with previous studies in Table I. It can be seen that our results are in good agreement with other studies. We note that the extrapolation of our earlier Wilson action data [31] gives generally less accurate scaling coefficients.

TABLE I: Results for the coefficients f_0 (slope of the scaling curve) and f_1 (the intercept of the scaling curve) in the weak-coupling limit for the antisymmetric mass gap.

Source	f_0	f_1
Villian (Hamiltonian) [8]	6.345	4.369
Plaquette Expansion [17]	5.01	5.82
Morningstar [12]	5.23	5.94
Hamer and Irving [9]	5.30	6.15
Hamer, Oitmaa and Weihong [10]	5.42	6.27
Heys and Stump [43]	4.97	6.21
Lana [44]	4.10	4.98
Xiyan, Jinming and Shuohong [15]	5.0	5.90
Dabringhaus, Ristig and Clark [14]	4.80	6.26
Darooneh and Maodarres [45]	4.40	5.78
Present Work	5.0(1)	5.8(1)

The finite size scaling behaviour of the mass gap [42] is shown as dashed line. It can be seen that finite size corrections do not dominate the mass gap until $\beta \geq 2.4$.

Figure 4 shows estimates of the scalar glueball mass in the Hamiltonian limit together with the results from previous series expansions [10] and quantum Monte Carlo calculation [1]. The graph shows an exponential behaviour of the glueball estimates in accordance with the behaviour predicted by theory. The solid line is a fit to the earlier series data over the range $1.0 \leq \beta \leq 2.0$. It can be seen that our present estimates agree well with the results from other studies [1, 10].

Finally, Figure 5 shows the behaviour of the dimensionless mass ratio²,

$$R_M = M_{0++}/M_{0--} \quad (14)$$

as a function of effective lattice spacing a_{eff} . At large β , the theory is expected to approach a theory of free bosons [8] so that the symmetric state is composed of two antisymmetric bosons and the mass ratio should approach

² As in the 4 dimensional confining theories, we may expect that quantities of this sort will approach their continuum limit with corrections of $O(1/a_{eff})$, where a_{eff} is the effective lattice spacing in ‘physical’ units when mass gap has been normalized to a constant. Hence for our present purpose we define $a_{eff} = \sqrt{8\pi^2\beta e^{-\pi^2\beta v(0)}}$ [8] with $v(0) = 0.3214$.

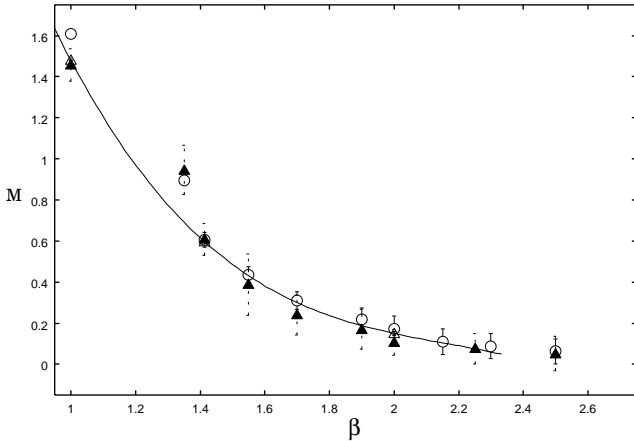


FIG. 4: Antisymmetric glueball mass as a function of β . The open circles show our present results. Our earlier results from Wilson action [31] and quantum Monte Carlo simulations [1] are shown as solid triangles and open triangles respectively. The solid line is a fit to the earlier data from series expansions [10].

two. The plot shows that as a_{eff} approaches to zero, the mass ratio approaches very closely to expected value of 2. A linear fit to the data from $0.014 \leq a_{eff} \leq 0.37$ gives $R_M = 1.98 \pm 0.06$, which is very close to our earlier Euclidean estimate [46]. However, we expect the Hamiltonian estimates to be less accurate than the Euclidean ones because of the large extrapolation involved. Using standard Wilson action, on the other hand, the Hamiltonian estimates of the mass ratio were hampered by errors and were virtually worthless.

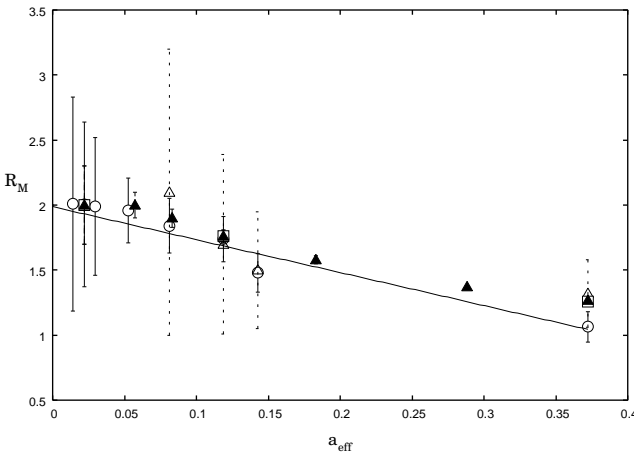


FIG. 5: Mass ratio, R_M , as a function of the effective lattice spacing, a_{eff} . Our present estimates are shown by the circles. The solid line is a linear fit to our data over the range $0.014 \leq a_{eff} \leq 0.37$. The open triangles show our previous estimates using the Wilson action [31]. The solid triangles and squares show the previous series [10] and quantum Monte Carlo [23] estimates respectively.

TABLE II: Results for the string tension K , symmetric and antisymmetric glueball masses M_{0++} , M_{0--} and the mass ratio R_M .

β	K	M_{0++}	M_{0--}	R_M
1.0	0.180(2)	1.7(1)	1.60(1)	1.0(1)
1.35	0.147(2)	1.31(9)	0.89(2)	1.4(1)
1.414	0.101(2)	1.05(4)	0.60(3)	1.7(1)
1.55	0.057(4)	0.80(4)	0.43(4)	1.8(2)
1.70	0.033(3)	0.59(4)	0.31(4)	1.9(2)
1.90	0.017(2)	0.42(7)	0.21(5)	1.9(5)
2.0	0.015	0.34(1)	0.17(6)	2.0(6)
2.15	0.010	0.22(1)	0.10(6)	2.0(1.0)
2.30	0.006	0.17(1)	0.08(6)	2.0(1.0)
2.50	0.005	0.12(1)	0.06(6)	

IV. CONCLUSION

In this paper we have studied the string tension and the mass gap of (2+1) dimensional U(1) lattice gauge theory. Using Euclidean path integral Monte Carlo methods on anisotropic lattices, the Hamiltonian limit of the model was obtained by extrapolating the to $\Delta\tau \rightarrow 0$ limit. The extrapolations to the Hamiltonian limit were performed by simple cubic fits. In this limit the string tension and antisymmetric mass gap show evidence of scaling in accordance with the asymptotic behaviour predicted by a weak-coupling approximation. In the naive continuum limit of the U(1) theory the string tension falls off exponentially with inverse lattice spacing, however, as a function of inverse coupling, which is all the Monte Carlo calculations care about, string tension behaves in a similar fashion to that of the 4-dimensional SU(N) lattice gauge theories

Our scaling coefficients for the antisymmetric mass gap agree well with earlier numerical studies. In the limit $a_{eff} \rightarrow 0$, the dimensionless mass ratio scales to a value near 2.0, as expected for a theory of free scalar bosons. A comparison with our earlier simulation data using Wilson action shows that more accurate determinations of the string tension, mass gap and dimensionless mass ratio have been achieved. Because of the large extrapolation needed, the estimates of the string tension and scalar glueball masses, in the Hamiltonian limit, were accompanied by errors, but these errors were half as large as those obtained using the standard Wilson action. This confirms the validity and efficiency of the mean-field improvement techniques.

These results clearly demonstrate that PIMC is an effective technique for obtaining reliable results in Hamiltonian formulation and provides an excellent alternative to other methods as was found in Refs. [31] and [32]. Although suffering the disadvantage of the extrapolation involved, PIMC method is a powerful tool and seems

to offers a more robust approach to Hamiltonian lattice gauge theories. In order to make the PIMC method a valuable tool in Hamiltonian lattice gauge theories, it is crucial to show that it allows to treat gauge theories and eventually matter fields, especially in non-Abelian case. If the PIMC techniques work for such theories, there is much interesting physics to be done, where conventional non-perturbative methods, in particular Lagrangian lattice field theory, have brought little progress.

We plan to use the path integral Monte Carlo techniques to Symanzik improved gauge action to test the effect of improved discretization on the scaling coefficients of the string tension and antisymmetric mass gap. We

shall report on these results in the near future. We also plan to study improved QCD in (3+1) dimensions and to explore Hamiltonian limit in that case.

Acknowledgments

This work was supported by the Australian Research Council. We are grateful for access to the computing facilities of the Australian Centre for Advanced Computing and Communications (ac3) and the Australian Partnership for Advanced Computing (APAC).

[1] C.J. Hamer, K. C. Wang and P. F. Price, Phys. Rev. **D50**, 4693 (1994)
[2] A.M. Polyakov, Nucl. Phys. **B120**, 120 (1977)
[3] A.M. Polyakov, Phys. Letts. **B72**, 477 (1978)
[4] H.R. Fiebig and R.M. Woloshyn, Phys. Rev. **D42**, 3520 (1990)
[5] T. Banks, R. Myerson and J. Kogut, Nucl. Phys. **B129**, 493 (1977)
[6] T. Banks, *et al.*, Phys. Rev. **D15**, 1111 (1978)
[7] S.D. Drell, H.R. Quinn, B. Svetitsky and M. Weinstein, Phys. Rev. **D19**, 619 (1979)
[8] M. Göpfert and G. Mack, Commun. Math. Phys. **82**, 545 (1982)
[9] C.J. Hamer and A.C. Irving, Z.Phys. **C27**, 145 (1985)
[10] C.J. Hamer, J. Oitmaa and Z. Weihong, Phys. Rev. **D45**, 4652 (1992)
[11] A.C. Irving, J.F. Owens and C.J.Hamer, Phys. Rev. **D28**, 2059 (1983)
[12] C.J. Morningstar, Phys. Rev. **D46**, 824 (1992)
[13] C.J.Hamer, Zheng Weihong and J. Oitmaa, Phys. Rev. **D53**, 1429 (1996)
[14] A. Dabringhaus, M.L. Ristig and J.W. Clark, Phys. Rev. **D43**, 1978 (1991)
[15] X.Y. Fang, J.M. Liu and S.H. Guo, Phys. Rev. **D53**, 1523 (1996)
[16] S.J. Baker, R.,F. Bishop and N.J. Davidson, Phys. Rev. **D53**, 2610 (1996).
[17] J. McIntosh and L. Hollenberg, Z. Phys. **C76**, 175 (1997)
[18] S. A. Chin, J. W. Negele and S. E. Koonin, Ann. Phys. (N.Y.) **157**, 140 (1984)
[19] S. E. Koonin, E. A. Umland and M. R. Zirnbauer, Phys. Rev. **D33**, 1795 (1986)
[20] C. M. Yung, C. R. Allton and C. J. Hamer, Phys. Rev. **D33**, 1795 (1986)
[21] A. Duncan and R. Roskies, Phys. Rev. **D31**, 364 (1985)
[22] E. Dagotto and A. Moreo, Phys. Rev. **D31**, 865 (1985)
[23] C.J. Hamer, R.J. Bursill and M. Samaras, Phys. Rev. **D62**, 054511 (2000)
[24] C.J. Hamer, R.J. Bursill and M. Samaras, Phys. Rev. **D62**, 074506 (2000)
[25] M. Creutz, L. Jacobs and C. Rebbi, Phys. Letts. **95**, 202 (1983)
[26] M. Creutz, Phys. Rev. Letts. **43**, 553 (1979)
[27] J. Sexton, A. Vaccarino and D. Weingarten, Phys. Rev. Letts. **75**, 4563 (1995)
[28] G. Boyd, *et al.*, Nucl. Phys. **B469**, 419 (1996)
[29] J.Li, S. Guo and X. Luo, Commun. Theor. Phys. **34**, 301 (2000)
[30] C. Morningstar and M. Peardon, Phys. Rev. **D 60**, 034509 (1999)
[31] M. Loan, M. Brunner, C. Sloggett and C. Hamer, Phys. Rev **D 68**, 034504 (2003)
[32] T. Byrnes, M. Loan, C. Hamer, F. Bonnet, D. Leinweber, A. Williams and J. Zanotti, to be published
[33] G.P. Lepage and P.B. Mackenzie, Phys.Rev. **D48**, 2250 (1993)
[34] T.R. Klassen, Nucl. Phys. **B533**, 557 (1998)
[35] G.P. Lepage, Nucl. Phys. **B (Prog. Suppl.)**, **60**, 267 (1998)
[36] C. Morningstar and M. Peardon, Nucl. Phys. **B (Prog. Suppl.)**, **47**, 258 (1996)
[37] C. Morningstar and M. Peardon, Phys. Rev. **D56**, 4043 (1997)
[38] P. Srianesh, C. Hamer and R. Bursill, Phys. Rev. **D62**, 034508 (2000)
[39] A.C. Irving and C.J. Hamer, Nucl. Phys. **B235**, 358 (1984)
[40] C.J. Hamer and Zheng Weihong, Phys. Rev. **D48**, 4435 (1993)
[41] M. Teper, Phys. Rev. **D59**, 014512 (1999)
[42] M. Weigel and W. Janke, Phys. Rev. Lett. **82**, 2318 (1999)
[43] D.W. Heys and D.R. Stump, Nucl. Phys. **B257**, 19 (1985)
[44] G.Lana, Phys. Rev. **D38**, 1954 (1988)
[45] A. Darooneh and M. Modarres, Eur. Phys. J. **C17** 169 (2000)
[46] M. Loan, T.Byrnes and C. Hamer, submitted to Eur. Phys. J. **C**